

1 **Fracture Imaging Using DAS-recorded Microseismic**  
2 **Events**

3 **Frantisek Stanek, Ge Jin, James L. Simmons**

4 Colorado School of Mines, Dept. of Geophysics, RCP, Golden, Colorado.

5 **Key Points:**

- 6 • Mapping fractures and understanding the reservoir response are the main goals  
7 of microseismic monitoring during hydraulic fracturing.  
8 • Distributed Acoustic Sensing provides high spatial resolution of microseismic re-  
9 flections data.  
10 • The proposed fracture imaging workflow uses reflected shear waves in the time-  
11 space domain to map induced fractures in space domain.

---

Corresponding author: Frantisek Stanek, [FStanek@mines.edu](mailto:FStanek@mines.edu)

Corresponding author: Ge Jin, [gjin@mines.edu](mailto:gjin@mines.edu)

## Abstract

Hydraulic fracturing enables hydrocarbon production from unconventional reservoirs. Mapping induced seismicity around newly created fractures is crucial for understanding the reservoir response and increasing the efficiency of operations. Distributed acoustic sensing (DAS) provides a large amount of high spatial resolution microseismic data acquired along the entire length of horizontal wells. We focus on the observed reflected S-waves and develop a new methodology to image induced fractures acting as reflectors in the media surrounding the events and monitoring fiber. The workflow consists of DAS data preprocessing, event location, wavefield separation, raytracing-based imaging, and image postprocessing. The comparison of the resulting fracture images with low-frequency DAS signals with fracture hits corroborates that the reflections are from fractures created by stimulation. The fracture imaging algorithm can be used for real-time mapping of fractures and tracking fracture changes in time. It leads to a better understanding of the reservoir response to hydraulic fracturing stimulation.

## Plain Language Summary

Hydraulic fracturing is a stimulation technique enabling hydrocarbon production from unconventional reservoirs. The high-pressure injection creates fractures and increases permeability in the reservoir. Small earthquakes (microseismic events) are induced around newly created fractures in the stimulated area. By using fiber-optic-based Distributed Acoustic Sensing technology, we can record seismic waveforms generated by the microseismic events with very high spatial resolution. We observed seismic energy scattered at the created hydraulic fractures and used the energy to image the hydraulic fractures' geometry. The newly developed methodology can be used for mapping induced hydraulic fractures. Knowledge of fractures, their geometry and position, is important for understanding the reservoir response to injection and potentially increasing the effectiveness of the following operations.

## 1 Introduction

Microseismic monitoring of hydraulic fracturing has been employed to understand the reservoir response and increase the efficiency of subsurface operations (Grechka & Heigl, 2017). Similarly, induced seismicity monitoring has been used during waste-water injection (e.g., Zoback, 2012), mining (e.g., Mendecki, Lynch, & Malovichko, 2010), enhancing of geothermal systems (e.g., Kwiatek, Bulut, Bohnhoff, & Dresen, 2014), storing gas underground (e.g., Carannante, D'Alema, Augliera, & Franceschina, 2020) and CO<sub>2</sub> sequestration (e.g., Williams-Stroud et al., 2020) to mitigate seismic hazard.

A commonly provided result of hydraulic fracturing microseismic monitoring is a catalogue of detected microseismic events with their origin time, location of hypocenter, magnitude and, if possible, a description of source mechanism. The main, and challenging, goal is to describe fracture geometry and orientation, connectivity between individual fractures, and estimate the area of the rock volume having increased permeability. The interpretation is mostly done with Discrete Fracture Network (Williams-Stroud et al., 2013), Stimulated Rock Volume (Rahimi Zeynal et al., 2014) and geomechanical models (e.g., Staněk & Eisner, 2017). However, due to uncertainties in event locations and inverted fault planes, and lack of understanding what microseismicity really represents, more accurate knowledge of induced fracture systems is still in need.

Another technique to map induced fractures, instead of connecting located events, is reflection imaging using microseismic events as sources. Grechka et al. (2017), Reshetnikov et al. (2010) or Lin and Zhang (2016) observed reflected waves in data acquired by 3C geophone arrays and used them for microseismic imaging. Such imaging is not common probably because it is difficult to see reflected waves in the microseismic data acquired by sparse geophone arrays.

Recently, distributed fiber optic sensing technology (Hartog, 2017) providing dense monitor-

ing data started to be employed in oil and gas industry as an alternative to the traditional seismic arrays. Fiber-optic-based monitoring is a quickly developing technology that has been used for measuring vibrations, temperature, and strain for many different purposes (e.g., Baldwin, 2015). Specifically, Distributed Acoustic Sensing (DAS) is being utilized for a long-term monitoring of vibrations. The fiber working as a sensor can be installed along the whole length of the stimulated well (in-well monitoring) or offset wells (cross-well monitoring). The best practice seems to be cementing fiber behind casing for permanent monitoring, although it can also be installed temporarily. Such monitoring geometry allows detection of a high number of weak (i.e., low magnitude) microseismic events due to proximity to the stimulated area. DAS offers other advantages compared to borehole geophone arrays, such as broadband response (from mHz to tens of kHz), long aperture (several km long fiber) and dense spatial sampling (channel spacing can be  $< 1$  m). The main downside of fiber-optic-based monitoring is a single-component axial strain measurement only in the direction along the fiber (Baird et al., 2019). This causes critical problems when locating and inverting source mechanism of microseismic event detected by a single fiber. However, there are ways to overcome this issue using multi-component, so called, helical optical fibers (Lim Chen Ning & Sava, 2018), monitoring carried out by deviated or L-shaped array (Verdon et al., 2020), or monitoring with two or more nearby fiber well(s) (e.g., Cole et al., 2018).

DAS provides high spatial resolution recordings enabling detailed analyses of wavefield and development of new processing methods leading to improved interpretations and better insight into the reservoir response. In passive seismic, we rely on induced microseismic events around the monitoring wells at a reasonable distance to detect them. Recorded waves (i.e., arrival times and amplitudes) contain information about event location relative to a monitoring array, radiation pattern due to source processes, and about the media between source and fiber. It includes also the structural features represented by reflected/refracted/diffracted waves arriving later after the direct body waves arrival (Lellouch & Biondi, 2021). In some DAS-based microseismic data, one may observe not only far-field but also near-field signal (Luo, Jin, & Stanek, 2021) which can be used for more precise source description, and dispersive guided waves providing properties of anomalous velocity layers and helping identification of events located inside or outside reservoir layer (Luo, Lellouch, et al., 2021). While all the phenomena are recorded with high resolution, we can not only map fracture propagation based on microseismic events located along fractures but also image fractures making use of reflected waves.

Another type of fiber-optic-based measurements during hydraulic fracturing used to describe fractures is low-frequency ( $< 1$  Hz) DAS (LFDAS). LFDAS measures strain changes (i.e., works as hybrid distributed strain sensing, DSS) induced by hydraulic fractures (Jin & Roy, 2017; Jin et al., 2021; Zhu & Jin, 2021). The detected strain signals represent fractures which were initiated at the offset well and reached the monitoring fiber well, so called fracture hits or frac-hits. Therefore, frac-hits are clear proof that the fractures have half-length longer than spacing between treatment and monitoring well. LFDAS data also shows time intervals when the fracture is opening (extension at the fracture and compression around) and when it is closing (extension around fracture) due to the leak-off after injection.

In this study, we analyze selected examples of field DAS-based microseismic data acquired during multi-well hydraulic fracturing, focused on observed reflected S-waves and propose a new method for imaging fractures in the vicinity of induced microseismic events. Imaged fractures are compared to LFDAS frac-hits to corroborate that the imaged waves are reflected from newly created hydraulic fractures.

## 2 Data and Methodology

### 2.1 DAS Data and Observations

We analyze data from the Chalk Bluff project in the Denver-Julesburg (DJ) Basin in Colorado, USA. Figure 1 shows a map of the study area with position of the pad of horizontal wells drilled in a N-S direction through the target unconventional reservoir formations

114 Codell and Niobrara at depths around 7400 - 7700 ft (TVD). The reservoir was hydraulically  
 115 fractured in hundreds of stages along lateral parts of all the horizontal wells. DAS microseis-  
 116 mic and LFDAS monitoring of the studied area was carried out by two fibers permanently  
 117 installed outside the casing of the red wells in Figure 1.

118 We have analyzed several strong microseismic events visible in the continuous DAS data.  
 119 The waveforms of most of the events are relatively simple with symmetrical moveouts of  
 120 direct P- and S-waves, where S-wave signals are usually higher amplitude than P-waves.  
 121 Here, we focus on three example events which have more complex wavefields. DAS data  
 122 and initial spatial locations (taken from catalogue of events located from surface array, pro-  
 123 vided by the data owner) of the selected events are shown in Figure 1 (yellow stars). Events  
 124 A and C have both clear direct P- and S-waves (marked as PD, SD), event B has only an  
 125 S-wave visible probably because of the lower magnitude. All three events have reflected  
 126 S-waves (marked as SR) but event C has a very complex wavefield following the S-wave  
 127 arrival. We also notice secondary, similarly looking, weaker events coming after and before  
 128 the main event in the data of the events A and B, respectively. These repeated events most  
 129 probably occurred at the same location as the main events but at slightly different times.

130 The observed reflected waves could represent either a fault, fracture, or velocity interface,  
 131 acting as a reflector in the medium around event location at the time when microseismic  
 132 event occurred. However, in our case, we can exclude the possibility of reflections from  
 133 near-horizontal interfaces (i.e., bedding planes) based on traveltimes moveout. Reflection  
 134 from a horizontal interface would be recorded by most of the channels along the fiber and  
 135 be symmetric around the apex with a moveout similarly to the direct P- and S-waves.  
 136 We interpret the reflected S-waves as reflections from approximately near-vertical faults, or  
 137 near-vertical fractures perpendicular to the horizontal fiber. Furthermore, the reflectors in  
 138 all three cases are most probably either very close to, or directly intersecting the fiber, as  
 139 we see that the arrivals of reflected S-waves and direct S-waves merge to the same channels  
 140 where the reflectors likely intersect with the fiber well.

## 141 2.2 Fracture reflection imaging - methodology

142 The reflected S-waves observed in the DAS data indicate the presence of reflectors in  
 143 the area between the event locations and the recording fiber. From the moveouts, we may  
 144 expect that the reflector orientation is near-vertical and perpendicular to horizontal well.  
 145 Our first attempt to explain reflected S-waves (Stanek & Jin, 2021) was simple traveltimes  
 146 modeling. We were able to fit manually picked arrival times of P-, S- and reflected S-waves  
 147 sufficiently well with synthetic traveltimes using a homogeneous isotropic velocity model  
 148 (velocity taken from an available sonic log) with a vertical reflector perpendicular to the  
 149 monitoring fiber well. However, such a method is not optimal as it requires testing of  
 150 many different positions, orientations, and lengths of reflector until synthetics fit the arrival  
 151 times.

152 Here, we propose an imaging technique converting DAS microseismic data in time to an  
 153 image with reflector position in space. The raytracing-based method is similar to that used  
 154 for DAS VSP processing (Schultz, 2019). The imaging procedure is incorporated into the  
 155 seven-step workflow (also shown in Figure 2):

156 (1) Input cut-out 0.3 s long chunk of DAS data containing detected event (as shown in  
 157 Figure 1) is pre-processed. We down-sample data from 10 kHz to 1 kHz sampling rate  
 158 in order to minimize data size and then apply a band-pass filter to preserve the signal of  
 159 interest between 10 and 300 Hz.

160 (2) We manually pick (P- and) S-wave arrivals and relocate the event using a standard  
 161 grid-search location algorithm minimizing the L1-misfit. This way we improve the origin  
 162 time and initial location taken from surface catalogue, specifically, the event location along  
 163 the fiber and perpendicular distance from the fiber. We cannot fully control the depth when  
 164 locating event using one-well DAS data due to the single-component nature of DAS.

165 (3) In this step the data are converted to f-k domain and the workflow splits into two parallel  
 166 branches. Steps (3a) and (3b), f-k filtering is used to remove downgoing (toe-ward going)

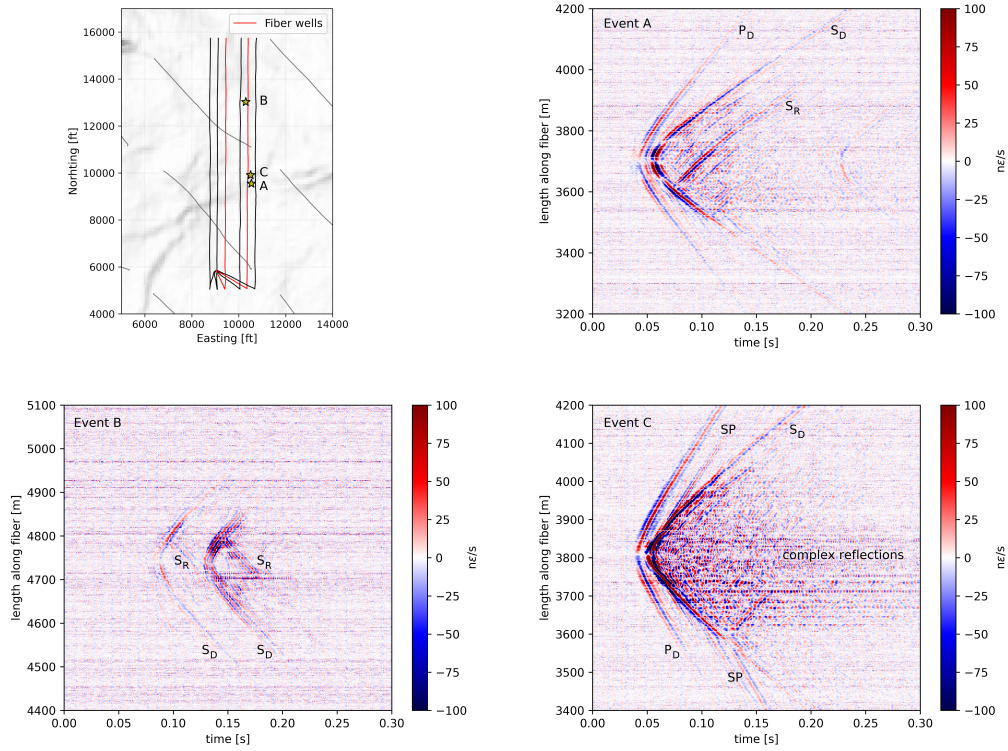


**Figure 1.** Upper left: A map of the horizontal wells (running N-S) and their relative positions. Wells with permanently installed fiber are shown in red. The diagonal NW-SE wells shown in gray are previously drilled production wells in the Niobrara. The yellow stars represent examples of strong microseismic events (A, B, C). The seismic coherency map in the background may indicate potential faults in the Niobrara formation. Upper right and bottom: Examples of three representative microseismic events with direct P-waves (PD), direct S-waves (SD), converted S- to P-waves (SP) and reflected S-waves (SR) recorded by DAS array. The events A and B are accompanied by another weaker event with very similar moveout indicating similar location but slightly different origin time. Event C shows more complicated reflections after the direct S-wave.

and the upgoing (heel-ward going) waves, respectively.

(4) To get rid of the remaining part of direct arrival body waves' moveouts, we mute all the data below (4a) and above (4b) the line going through the apex with the slope equal to S-wave velocity (muted areas are highlighted by transparent orange triangles in Figure 2). This line needs to be slightly shifted relatively to the apex to make sure that we fully mute the direct S-waves and do not deteriorate final image. After the latter step we should see only upgoing or downgoing reflected waves.

(5) The idea of imaging in (5a) and (5b) of the workflow is that every point between the fiber at  $x = 0$  and the event location  $[x_s, 0]$  acts as a potential reflection point  $[x_f, y_f]$ . With an assumption that the reflector is almost vertical and perpendicular to fiber, we compute the raytracing-based travel time of the reflected S-wave  $tt$  in a homogeneous isotropic velocity model with S-wave velocity  $V_S$ :

$$tt = \frac{2y_f - y_r}{V_s}. \quad (1)$$

The channel  $y_r$  along the fiber where the ray of reflected wave arrives is:

$$y_r = x_s - \left( y_f - \frac{x_f y_f}{x_s - x_f} \right). \quad (2)$$

DAS data amplitude from the channel  $y_r$  at the time  $tt$  is then assigned to the tested reflection point in space. After going through all the potential reflection points between the fiber and the event location the imaging is done.

The final two steps are: (6) merging the two images of downgoing and upgoing reflected waves to form a complete image and (7) post-processing. Here, we calculate signal envelopes and apply a low-pass filter to the merged image to further enhance visibility of reflector(s). An example of the resulting image is shown at the bottom of workflow where the dark color means no reflection or data coverage, and coherent near-horizontal bright spots represent positions of near-vertical reflectors approximately perpendicular to the fiber.

### 3 Results

#### 3.1 Imaged Reflectors

We demonstrate the processing results for two microseismic events (Events A and B as displayed in Figure 1) using the above-described methodology. Figure 3 shows input DAS microseismic waveforms and the resulting images of reflectors in space in two columns on the left. Each image is a 2D plane between the event location and the part of fiber from which we have DAS data.

The bright spots elongated in the direction approximately perpendicular to fiber indicate the imaged reflectors. The length of imaged reflectors is proportional to the length of reflected wave visible in the DAS data. The imaged reflectors usually do not intersect with the fiber (at the distance 0) because of the mute window around the direct arrivals (including a few wavelengths of high amplitude S-wave coda). The muting must be done to avoid distortion of the final image around apex. However, we realize that we also mute part of the reflected S-wave signal mixed with S-wave coda and thus lose information about the reflector in the vicinity of the fiber. The imaged reflectors fade out with distance from fiber similarly like the signal of reflected wave in DAS data, probably due to attenuation and larger channel offset. It does not mean that the reflectors are not longer, as we image only its visible parts illuminated by the individual microseismic event. The black color at the far distance from the fiber means no data coverage, i.e., there are no points reflecting energy back to the part of fiber we have data from. Whereas the black spaces in a narrow zone around the apex line result from muting the direct S-wave in the input data (steps (4a) and (4b) of the workflow). All the other spaces with dark colors are representing media without reflectors.

The image of Event A shows one very clear horizontal bright spot representing a reflector within 50 m from the fiber. In the DAS data, the position of imaged reflector along the fiber is corresponding to the channel where both direct S- and reflected S-waves intersect (highlighted by green dashed-line arrow in the Figure 3). There is another reflector in the

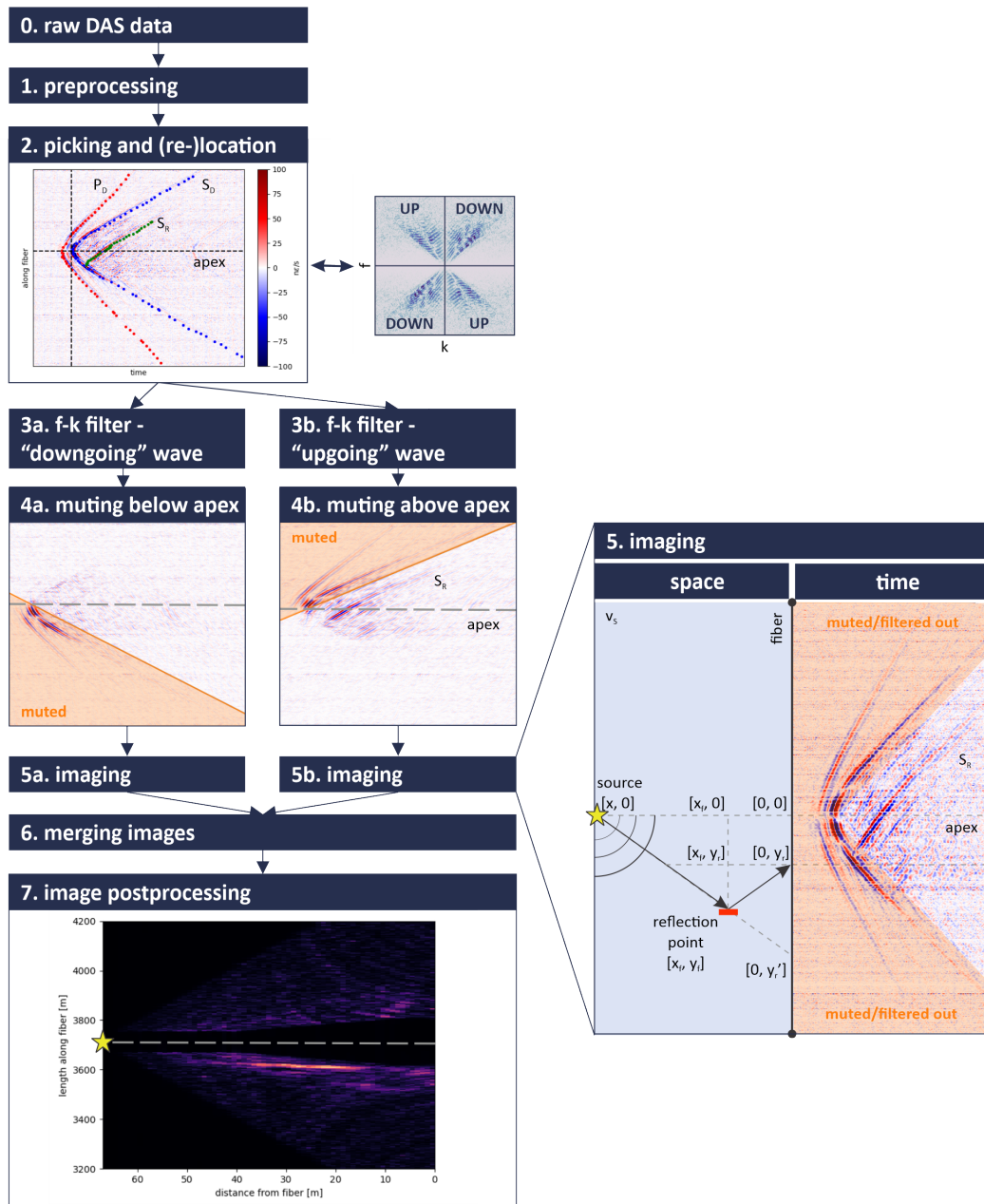


**Figure 2.** Proposed 7-step workflow of reflector imaging using reflected S-waves recorded by DAS with an illustration of raytracing-based reflector imaging methodology.

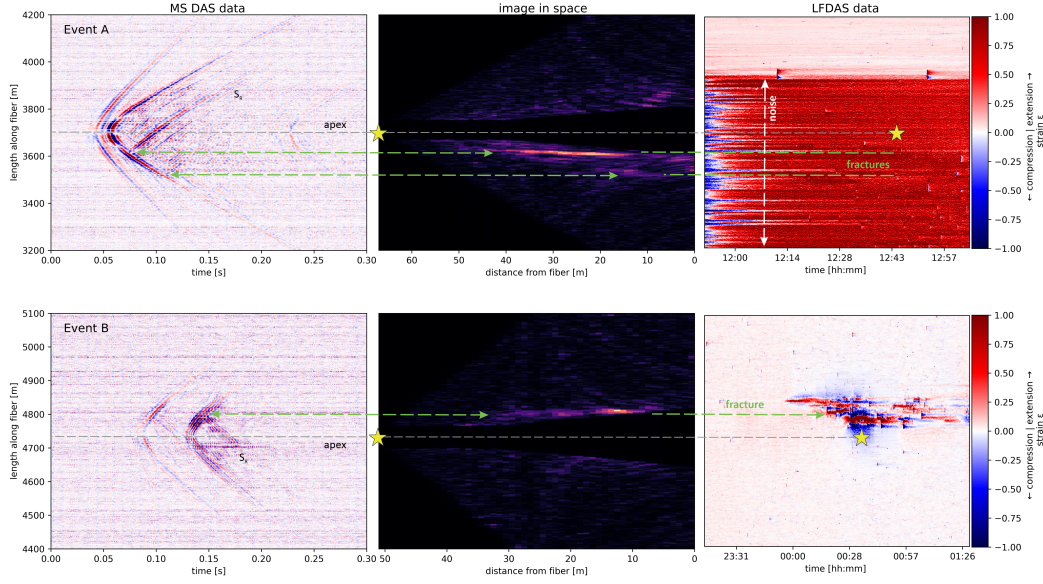


**Figure 3.** Input DAS data, reflector images and LFDAS data for two example events. The green dashed-line arrows highlight position of reflectors in the images. The yellow stars represent location and origin time (only in the LFDAS data) of microseismic events.

218 image which is weaker and shorter (visible within 20 m from the fiber) than the main reflector  
 219 but still with coherent brightness in the direction from fiber. The matching reflected S-wave  
 220 in the DAS data is of proportionally low signal-to-noise ratio (SNR) and its amplitude  
 221 quickly attenuates away from the fiber. The remaining randomly located bright spots are  
 222 too small and probably result from coherent noise in the input data. Meanwhile, Event B  
 223 has one approximately 30 m long reflector visible in its image.

### 224 3.2 Comparison with LFDAS and interpretation

225 Up to this point, we have referred to bright spots in images as reflectors because we  
 226 had no clear indication of whether they can be interpreted as newly created fractures due  
 227 to hydraulic fracturing or pre-existing vertical faults in the area. To inspect whether we  
 228 image one or the other we compare the images with LFDAS data. The LFDAS data are  
 229 the same recorded raw DAS data as the analyzed DAS microseismic data but in a very  
 230 low frequency band ( $< 0.1$  Hz). Figure 3 shows images for both microseismic events in  
 231 the middle and LFDAS data from the corresponding stage in the right column. The yellow stars  
 232 placed in the LFDAS data are at the events' origin time and location along the fiber. Note  
 233 that the DAS microseismic data of each event and consequently the image of reflector(s)  
 234 is a snapshot of the medium around the event location at the time when event happened,  
 235 whereas the LFDAS data show evolution of measured strain during the entire stage.  
 236 The LFDAS data around the origin time and location of the Event B shows a very clear  
 237 signal characteristic of frac-hits. The first fracture started to open (zone of compression  
 238 in blue around the extensive opening zone in red) shortly before 12 am. Later on, other  
 239 fractures hit the fiber approximately 80 m aside of the first frac-hit and started to open.  
 240 A few minutes later, the changes in the reservoir induced Event B recorded by DAS array.  
 241 The comparison with LFDAS provides undeniable evidence that the observed S-wave is  
 242 back-scattered from the newly created fracture to the monitoring fiber - position of fracture  
 243 in our image aligns with the position of frac-hit in the LFDAS data (see the green dashed-  
 244 line arrow). The explanation why we identified only one fracture in the image while the

245 LFDAS shows three existing fractures at the event origin time is unclear. It is less likely to  
 246 be resolution issue as the thickness of imaged fracture is smaller than the entire fractured  
 247 zone. The first opened fracture (at the top in the LFDAS) is most likely not imaged due  
 248 to its narrower width or because the fracture was already closed and did not create enough  
 249 seismic impedance. The third fracture (at the bottom in the LFDAS) lies in the muted zone  
 250 of our image (too close to the apex of microseismic event).

251 The LFDAS data for the stage of hydraulic fracturing when the Event A occurred is of low  
 252 quality, not allowing detection of frac-hits. The source of abnormally high low-frequency  
 253 noise was an injection operation taking place in the monitoring well. This caused large  
 254 temporal change of temperature conditions short time before the LFDAS data was acquired.  
 255 Note that the low frequency noise does not affect the DAS microseismic data while we look  
 256 at much higher frequencies where the sensitivity to temperature is negligible. As the image  
 257 of Event B has been proven to be showing induced fracture(s), we may expect that the  
 258 similarly looking reflectors in the image of Event A are also fracture. However, we cannot  
 259 prove it by comparison with frac-hit due to the noisy LFDAS.

## 260 4 Discussion

### 261 4.1 Methodology

262 Our methodology relies on recorded signal reflected from fractures. We have used  
 263 reflected S-waves, but analogically reflected P-waves might be used. Visibility of reflected  
 264 waves in data depends on sensitivity of DAS monitoring system, magnitude of microseismic  
 265 event and relative geometry between source, fiber and fracture. If the microseismic event is  
 266 located too close to the induced fracture (relative to distance of the event from the fiber),  
 267 most of the energy is reflected to far offset channels (far from apex line in the DAS data)  
 268 and the signal of the reflected wave arrives shortly after direct body wave and has almost  
 269 the same moveout. Therefore, in our workflow, the reflected wave may be filtered out or  
 270 muted together with the body wave signal and information about fracture is lost. Remaining  
 271 energy reflected from the fracture appears close to the apex where it is usually mixing with  
 272 high SNR body-wave coda which we also mute. This means that fracture imaging using  
 273 reflected waves is hardly possible when the event-fracture-fiber geometry does not lead to a  
 274 reflected signal clearly distinguishable from signal of direct body waves.

275 Our fracture imaging methodology is based on several assumptions. The raytracing is done  
 276 only for reflections from a vertical fracture oriented approximately perpendicular to fiber  
 277 in a homogenous isotropic velocity model. These assumptions appear to be valid in that  
 278 the fractures are near vertical, and the events and monitor well are in the same horizontal  
 279 formation which can be described by a single velocity structure. Similar conditions might  
 280 be found in many other fields but, in general, to be able image fractures with arbitrary  
 281 orientation in a complex velocity model, we would need to use more sophisticated raytracing  
 282 or advanced imaging methods such as Kirchhoff migration or reverse time migration (e.g.,  
 283 Li et al., 2020). However, that would require more accurate event locations and stacking of  
 284 many microseismic events (sources) to get a reasonable image.

285 One of our first steps in the workflow is manual picking and event (re-)location as we wanted  
 286 to improve the initial event locations obtained from surface microseismic catalog. Without  
 287 the known initial location, we would also locate the event but have only information about  
 288 the event position along the fiber and distance from the fiber when located from one fiber  
 289 only. The event location would have uncertainty a  $360^\circ$  around the axis of the horizontal  
 290 well because of the axial sensitivity of DAS. Therefore, we would not know the correct  
 291 orientation of imaged fractures. Note that the image is always in the plane between the  
 292 event and the fiber. Of course, P- and S-wave arrivals needed for location do not have to  
 293 be picked manually if an efficient auto-picking algorithm is employed.

## 4.2 Application

The most obvious application of the fracture imaging is processing of continuous cross-well DAS microseismic data acquired during hydraulic fracturing to map created fractures around stimulated wells. Such detailed map can have big impact on precision of DFN and its reliability. With fracture imaging we may potentially map dynamic evolution of the fracture if several microseismic events are induced and detected during the same stage around the fracture. The microseismic events provide snapshots of the surrounding reservoir at their origin times. If we are able to image fractures, it means that the fracture is already open and wide enough to reflect energy from microseismic event. With several microseismic events following each other in time, we may see fracture growth, i.e., dynamic changes of the reflected wave visible in DAS data, and thus the lateral extent of the imaged fractures. When the fracture starts closing, seismic impedance decreases, and fracture disappears from image. Fracture closing was shown in LFDAS data by Jin and Roy (2017) as well as in time-lapse DAS VSP. Compared to the 4D inter-stage DAS VSP (Binder et al., 2020; Titov et al., 2021), our fracture imaging provides a better resolution due to higher frequency content (microseismic event as a source is closer to the fiber than surface source used for VSP) and can image fractures in 3D if the event location is known.

LFDAS monitoring has been used to monitor frac-hits. Unfortunately, as shown on example in Figure 3, LFDAS can be contaminated by noise due to temperature effects induced by injection operations in the monitor well. In such cases, fracture imaging of DAS microseismic data may provide complementary information to results from LFDAS. Furthermore, the LFDAS can detect frac-hits or strain changes only in the close vicinity of the monitoring fiber. Our fracture imaging is also able to map these frac-hits and, moreover, it has a capability to map fractures which do not intersect monitoring fiber well as the imaging space locates between the event and the monitoring fiber. From such images we can estimate fracture geometry of fractures with half-length shorter than well spacing. Of course, the disadvantage is that fracture imaging is dependent on induced microseismic events whereas LFDAS not.

## 5 Conclusions

We have shown examples of microseismic events recorded by DAS fiber in a horizontal well during hydraulic fracturing of unconventional reservoir. Besides direct P- and S-waves, the events have clearly visible signals of S-waves reflected at hydraulic fractures. We developed a new processing workflow to image the fracture using the reflected waves and demonstrated the conversion of DAS-based microseismic data in time to fracture image in space. Resulting images were compared to frac-hit signal in corresponding LFDAS data, supporting that the imaged reflectors are newly created hydraulic fractures. The fracture imaging can be further developed with a potential to be used for a real-time 3-D hydraulic fracture mapping when DAS monitoring is employed and induced microseismic events detected in abundance.

## Acknowledgments

This work was conducted with the support of the Reservoir Characterization Project (Phase XVIII.) at the Colorado School of Mines. The authors are thankful to Bonanza Creek Energy, Inc. for support, providing the data and permission to publish the results. Authors thank Alicia Downard for helping with orientation in the data and providing coherence maps, and Xiaoyu (Rosie) Zhu for helping with the LFDAS data. The DAS microseismic data of events A and B used as examples for fracture imaging in this study are available.

## References

- Baird, A., Stork, A., Horne, S., Naldrett, G., Kendall, M., Wookey, J., . . . Verdon, J. (2019). Modelling of Fibre-Optic DAS Response to Microseismic Arrivals in Anisotropic Media. In *81st EAGE Conference and Exhibition 2019* (pp. 1–6). London, UK.; European Association of Geoscientists & Engineers. doi: 10.3997/2214-4609.201901244
- Baldwin, C. S. (2015). Applications for fiber optic sensing in the upstream oil and gas industry. In G. Pickrell, E. Udd, & H. H. Du (Eds.), (p. 94800D). Baltimore, Maryland, United States. doi: 10.1117/12.2176226
- Binder, G., Titov, A., Liu, Y., Simmons, J., Tura, A., Byerley, G., & Monk, D. (2020). Modeling the seismic response of individual hydraulic fracturing stages observed in a time-lapse distributed acoustic sensing vertical seismic profiling survey. *Geophysics*, *85*(4), T225–T235. doi: 10.1190/geo2019-0819.1
- Carannante, S., D’Alema, E., Augliera, P., & Franceschina, G. (2020). Improvement of microseismic monitoring at the gas storage concession “Minerbio Stocaggio” (Bologna, Northern Italy). *Journal of Seismology*, *24*(5), 967–977. doi: 10.1007/s10950-019-09879-2
- Cole, S., Karrenbach, M., Kahn, D., Rich, J., Silver, K., & Langton, D. (2018). Source parameter estimation from DAS microseismic data. In *SEG Technical Program Expanded Abstracts 2018* (pp. 4928–4932). Anaheim, California: Society of Exploration Geophysicists. doi: 10.1190/segam2018-2995716.1
- Grechka, V., & Heigl, W. M. (2017). *Microseismic Monitoring*. Society of Exploration Geophysicists. doi: 10.1190/1.9781560803485
- Grechka, V., Li, Z., Howell, B., Garcia, H., & Wooltorton, T. (2017). High-resolution microseismic imaging. *The Leading Edge*, *36*(10), 822–828. doi: 10.1190/tle36100822.1
- Hartog, A. H. (2017). *An Introduction to Distributed Optical Fibre Sensors*. Boca Raton: CRC Press. doi: 10.1201/9781315119014
- Jin, G., & Roy, B. (2017). Hydraulic-fracture geometry characterization using low-frequency DAS signal. *The Leading Edge*, *36*(12), 975–980. (Publisher: Society of Exploration Geophysicists) doi: 10.1190/tle36120975.1
- Jin, G., Ugueto, G., Wojtaszek, M., Guzik, A., Jurick, D., & Kishida, K. (2021). Novel Near-Wellbore Fracture Diagnosis for Unconventional Wells Using High-Resolution Distributed Strain Sensing during Production. *SPE Journal*, *26*(05), 3255–3264. doi: 10.2118/205394-PA
- Kwiatak, G., Bulut, F., Bohnhoff, M., & Dresen, G. (2014). High-resolution analysis of seismicity induced at Berlin geothermal field, El Salvador. *Geothermics*, *52*, 98–111. doi: 10.1016/j.geothermics.2013.09.008
- Lellouch, A., & Biondi, B. L. (2021). Seismic Applications of Downhole DAS. *Sensors*, *21*(9), 2897. doi: 10.3390/s21092897
- Li, L., Tan, J., Schwarz, B., Staněk, F., Poiata, N., Shi, P., . . . Gajewski, D. (2020). Recent Advances and Challenges of Waveform-Based Seismic Location Methods at Multiple Scales. *Reviews of Geophysics*, *58*(1), e2019RG000667. doi: 10.1029/2019RG000667
- Lim Chen Ning, I., & Sava, P. (2018). High-resolution multi-component distributed acoustic sensing: Hi-res multi-component DAS. *Geophysical Prospecting*, *66*(6), 1111–1122. doi: 10.1111/1365-2478.12634
- Lin, Y., & Zhang, H. (2016). Imaging hydraulic fractures by microseismic migration for downhole monitoring system. *Physics of the Earth and Planetary Interiors*, *261*, 88–97. doi: 10.1016/j.pepi.2016.06.010
- Luo, B., Jin, G., & Stanek, F. (2021). Near-field strain in distributed acoustic sensing-based microseismic observation. *Geophysics*, *86*(5), P49–P60. doi: 10.1190/geo2021-0031.1
- Luo, B., Lellouch, A., Jin, G., Biondi, B., & Simmons, J. (2021). Seismic inversion of shale reservoir properties using microseismic-induced guided waves recorded by distributed acoustic sensing. *Geophysics*, *86*(4), R383–R397. doi: 10.1190/geo2020-0607.1
- Mendecki, A. J., Lynch, R. A., & Malovichko, D. A. (2010). Routine Micro-Seismic Monitoring in Mines. *Seismic Monitoring in Mines*, 33.

- 396 Rahimi Zeynal, A., Snelling, P., Neuhaus, C. W., & Mueller, M. (2014). Correlation of  
397 Stimulated Rock Volume from Microseismic Pointsets to Production Data - A Horn  
398 River Case Study. *OnePetro*. doi: 10.2118/169541-MS
- 399 Reshetnikov, A., Kummerow, J., Buske, S., & Shapiro, S. A. (2010). Microseismic imaging  
400 from a single geophone: KTB. In *SEG Technical Program Expanded Abstracts 2010*  
401 (pp. 2070–2074). Society of Exploration Geophysicists. doi: 10.1190/1.3513252
- 402 Schultz, W. (2019). *Time-lapse multicomponent geophone and DAS VSP processing and*  
403 *analysis*. (Unpublished master’s thesis). Colorado School of Mines, dept. of Geo-  
404 physics.
- 405 Stanek, F., & Jin, G. (2021). Reservoir characterization using DAS microseismic events. In  
406 *First International Meeting for Applied Geoscience & Energy Expanded Abstracts* (pp.  
407 463–467). Society of Exploration Geophysicists. doi: 10.1190/segam2021-3583216.1
- 408 Stanek, F., & Eisner, L. (2017). Seismicity Induced by Hydraulic Fracturing in Shales: A  
409 Bedding Plane Slip Model. *Journal of Geophysical Research: Solid Earth*, *122*(10),  
410 7912–7926. doi: 10.1002/2017JB014213
- 411 Titov, A., Binder, G., Liu, Y., Jin, G., Simmons, J., Tura, A., . . . Yates, M. (2021). Modeling  
412 and interpretation of scattered waves in interstage distributed acoustic sensing vertical  
413 seismic profiling survey. *Geophysics*, *86*(2), D93–D102. doi: 10.1190/geo2020-0293.1
- 414 Verdon, J. P., Horne, S. A., Clarke, A., Stork, A. L., Baird, A. F., & Kendall, J.-M. (2020).  
415 Microseismic monitoring using a fibre-optic Distributed Acoustic Sensor (DAS) array.  
416 *Geophysics*, 1–48. doi: 10.1190/geo2019-0752.1
- 417 Williams-Stroud, S., Ozgen, C., & Billingsley, R. L. (2013). Microseismicity-constrained dis-  
418 crete fracture network models for stimulated reservoir simulation. *Geophysics*, *78*(1),  
419 B37–B47. doi: 10.1190/geo2011-0061.1
- 420 Williams-Stroud, S., Bauer, R., Leetaru, H., Oye, V., Stanek, F., Greenberg, S., & Langet,  
421 N. (2020). Analysis of Microseismicity and Reactivated Fault Size to Assess the Potent-  
422 tial for Felt Events by CO<sub>2</sub> Injection in the Illinois Basin. *Bulletin of the Seismological*  
423 *Society of America*, *110*(5), 2188–2204. doi: 10.1785/0120200112
- 424 Zhu, X., & Jin, G. (2021). Analysis of cross-well fracture hits in DJ Basin, Colorado using  
425 low-frequency DAS data. In *First International Meeting for Applied Geoscience &*  
426 *Energy Expanded Abstracts* (pp. 457–462). Society of Exploration Geophysicists. doi:  
427 10.1190/segam2021-3582658.1
- 428 Zoback, M. D. (2012). Managing the Seismic Risk Posed by Wastewater Disposal. *Earth*  
429 *Magazine*, *57*(4), 38–43.